Slk19 clusters kinetochores and facilitates chromosome bipolar attachment

Daniel Richmond, Raed Rizkallah, Fengshan Liang, Myra M. Hurt, and Yanchang Wang
Department of Biomedical Sciences, College of Medicine, Florida State University, Tallahassee, FL 32306

ABSTRACT **In all eukaryotic cells, DNA is packaged into multiple chromosomes that are linked to microtubules through a large protein complex called a kinetochore. Previous data show that the kinetochores are clustered together during most of the cell cycle, but the mechanism and the biological significance of kinetochore clustering are unknown. As a kinetochore protein in budding yeast, the role of Slk19 in the stability of the anaphase spindle has been well studied, but its function in chromosome segregation has remained elusive. Here we show that Slk19 is required for kinetochore clustering when yeast cells are treated with the microtubule-depolymerizing agent nocodazole. We further find that *slk19*Δ mutant cells exhibit delayed kinetochore capture and chromosome bipolar attachment after the disruption of the kinetochore–microtubule interaction by nocodazole, which is likely attributed to defective kinetochore clustering. In addition, we show that Slk19 interacts with itself, suggesting that the dimerization of Slk19 may mediate the interaction between kinetochores for clustering. Therefore Slk19 likely acts as kinetochore glue that clusters kinetochores to facilitate efficient and faithful chromosome segregation.**

Monitoring Editor
Orna Cohen-Fix
National Institutes of Health

Received: Jul 26, 2012
Revised: Dec 20, 2012
Accepted: Dec 21, 2012

INTRODUCTION

An eukaryotic cell contains multiple chromosomes, but the centromeric regions from these chromosomes have been shown to be grouped together in yeast and human cells (Funabiki *et al.*, 1993; Goh and Kilmartin, 1993; Goshima and Yanagida, 2000; Solovei *et al.*, 2004; Duan *et al.*, 2009). In budding yeast, chromosomes are connected to microtubules and form clusters during most of the cell cycle (Goshima and Yanagida, 2000; Tanaka *et al.*, 2007; Liu *et al.*, 2008). Previous work shows that the centromere clustering in yeast cells is reduced in kinetochore mutants (Jin *et al.*, 2000; Janke *et al.*, 2001; Anderson *et al.*, 2009). One explanation is that kinetochore clustering is maintained by the association of kinetochores with microtubules. Recent evidence suggests that kinesin-5 sliding motor proteins Cin8 and Kip1 promote kinetochore clustering during mitosis by controlling the dynamics of kinetochore microtubules (Gardner *et al.*, 2008). Another motor protein, Kip3, is also involved in kinetochore clustering at metaphase (Wargacki *et al.*, 2010). However, the molecular mechanism for kinetochore clustering during other cell cycle stages and the biological function of this clustering remain unclear.

The budding yeast *SLK19* gene was isolated because the loss of its function causes lethality in cells lacking a motor protein Kar3. Given the fact that Kar3 promotes chromosome biorientation (Liu *et al.*, 2011; Jin *et al.*, 2012), the genetic interaction suggests a possible kinetochore function for Slk19. Indeed, Slk19 has been shown to associate with centromeric DNA (Zeng *et al.*, 1999; Zhang *et al.*, 2006). As a kinetochore protein, Slk19 is not essential for growth, and *slk19*Δ mutant cells show almost normal chromosome segregation kinetics compared with wild-type (WT) cells (Sullivan and Uhlmann, 2003; Jin *et al.*, 2008). Nevertheless, *slk19*Δ mutant is lethal in the absence of the spindle assembly checkpoint that monitors flawed kinetochore–microtubule (KT-MT) interactions, indicating the role of Slk19 in faithful chromosome segregation (Tong *et al.*, 2004; Ye *et al.*, 2005; Collins *et al.*, 2007). However, the kinetochore function of Slk19 has remained as a mystery at the molecular level.

This article was published online ahead of print in MBoC in Press (http://www.molbiolcell.org/cgi/doi/10.1091/mbc.E12-07-0552) on January 2, 2013.

Address correspondence to: Yanchang Wang (yanchang.wang@med.fsu.edu).

Abbreviations used: KT-MT, kinetochore-microtubule; WT, wild type; YPD, yeast peptone dextrose.

Slk19 is also a component of a mitotic exit pathway FEAR (Cdc14 early-anaphase release), which promotes the release of the phosphatase Cdc14 from the nucleolus during early anaphase. In addition to Slk19, the FEAR pathway includes separase Esp1, protein phosphatase 2A, Spo12, Fob1, and the polo-like kinase Cdc5 (Stegmeier *et al.*, 2002; Queralt *et al.*, 2006; Wang and Ng, 2006; Yellman and Burke, 2006). The FEAR-induced Cdc14 release reverses the protein phosphorylation imposed by S-phase CDK (cyclin-dependent kinase), which facilitates spindle elongation (Jin *et al.*, 2008). Moreover, Slk19 localizes to the spindle midzone during anaphase, where it stabilizes the spindle (Pereira and Schiebel, 2003; Khmelinskii *et al.*, 2007). Similar to the cohesin subunit Scc1/Mcd1, Slk19 is cleaved by separase Esp1 upon anaphase onset, and this cleavage is essential for Slk19's spindle-midzone localization (Sullivan *et al.*, 2001). A series of *slk19* in-frame deletion mutants was identified, and they are defective for either FEAR signaling or kinetochore function. Deletion of a fragment at the central region of *SLK19* leads to the synthetic lethality with *kar3* mutant without disrupting the FEAR function, suggesting the kinetochore-specific role of this region (Havens *et al.*, 2010).

Here we show that the absence of a yeast kinetochore protein Slk19 leads to kinetochore declustering after treatment with nocodazole, a microtubule-depolymerizing agent, even though untreated *slk19*Δ mutant cells exhibit normal kinetochore clustering. *slk19*Δ mutants exhibit normal chromosome segregation during an undisturbed cell cycle, but we observed a dramatic anaphase entry delay after nocodazole treatment. Data with live-cell imaging indicate that *slk19*Δ mutant cells exhibit defects in both kinetochore capture and chromosome biorientation. Our observation that Slk19 directly interacts with itself supports a possibility that Slk19 dimerization mediates kinetochore–kinetochore interaction and clustering, which likely facilitates kinetochore capture and chromosome bipolar attachment, especially after the disruption of kinetochore–microtubule interaction.

RESULTS

Kinetochore clustering is resistant to nocodazole treatment

Budding yeast kinetochores have been shown to form clusters (Goh and Kilmartin, 1993; Goshima and Yanagida, 2000). We confirmed the cluster formation in live cells with green fluorescent protein (GFP)–tagged Mtw1, a protein located in the center portion of the kinetochore (De Wulf *et al.*, 2003). Kinetochores form a single cluster before metaphase and appear as two clusters, presumably after the establishment of chromosome bipolar attachment (Supplemental Figure S1). To examine whether this clustering depends on KT-MT interaction, we examined the kinetochore distribution in cells that were first synchronized in preanaphase and then treated with nocodazole, a microtubule-depolymerizing drug. *cdc13-1* mutant cells arrest in preanaphase when incubated at nonpermissive temperatures due to the activation of the DNA-damage checkpoint by unprotected telomeres (Liang and Wang, 2007). Cells in *cdc13-1* background were first incubated at 34°C to achieve preanaphase arrest. After nocodazole treatment, *cdc13-1 MTW1-GFP SPC42-mApple* cells showed two adjacent spindle poles (Spc42-mApple). However, kinetochores marked by Mtw1-GFP formed a ring-like structure with two Spc42-mApple dots residing at each side of the ring (Figure 1A). Because the two spindle poles are still separated, and the Mtw1-GFP foci are in very close proximity to the spindle poles, we speculate that the nocodazole treatment of cells arrested in preanaphase cannot disrupt the KT-MT interaction completely. One possibility is that nocodazole-mediated microtubule depolymerization fails to disrupt some KT-MT interactions once they are established. If that is the case, we need to treat cells with nocodazole before the establishment of KT-MT interaction in order to disconnect kinetochores from microtubules more efficiently.

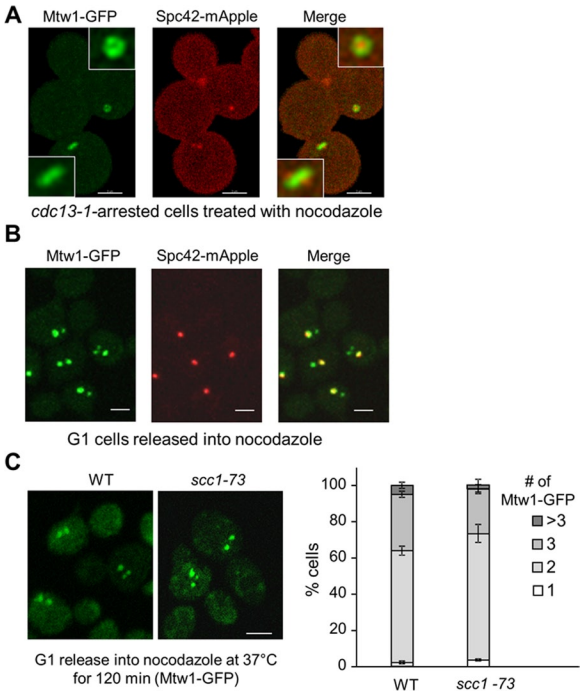

FIGURE 1: Kinetochores can form clusters in the absence of KT-MT interaction and sister-chromatid cohesion. (A) Most of the kinetochores remain connected to spindle poles after nocodazole treatment in cells first arrested in preanaphase. G_1-arrested *cdc13-1 MTW1-GFP SPC42-mApple* cells were released into YPD medium at 34°C for 120 min to achieve preanaphase arrest. Nocodazole was then added into the medium to 20 μg/ml, and the cells were harvested and fixed after 45 min of incubation at 34°C. Confocal microscopy was used to project a maximum-intensity image. Bar, 3 μm. (B) Some kinetochore clusters are disconnected from the spindle poles after G_1-arrested cells are released into nocodazole. G_1-arrested *MTW1-GFP SPC42-mApple* cells were released into medium containing 20 μg/ml nocodazole. After 120 min of incubation at 25°C, cells were fixed and subjected to confocal microscopy. Scale bar, 3 μm. (C) Kinetochore clustering after nocodazole treatment is normal in cohesin mutants. WT and *scc1-73* cells with *MTW1-GFP* were grown to log phase at permissive temperatures. After G_1 arrest, the cells were released into 37°C medium containing 20 μg/ml nocodazole for 120 min. More than 100 cells were counted for the number of Mtw1-GFP foci per cell for each sample, and the average from triplicates is shown (right). Left, representative images acquired by confocal microscopy. Scale bar, 3 μm.

When centromeric DNA is being duplicated by the replication machinery, kinetochore proteins are displaced from the centromere, which disrupts the KT-MT interaction (Kitamura *et al.*, 2007). Cells can replicate their DNA in the presence of nocodazole, but the reassembled kinetochores may fail to reestablish the connection to microtubules due to repressed microtubule polymerization by nocodazole. Therefore we released G_1-arrested yeast cells with Mtw1-GFP and Spc42-mApple into nocodazole (20 μ/ml) for 120 min, a condition that allows DNA synthesis but prevents microtubule polymerization. We examined the kinetochore distribution in these cells and found that most cells exhibited two or three GFP foci that mark kinetochores. Of interest, only one of the GFP dots colocalized with the collapsed spindle poles (Spc42-mApple) and others appeared to

float away from the spindle poles, indicating that some kinetochores are not connected to microtubules (Figure 1B). In most of the cases, mApple-marked spindle poles colocalize with the bigger GFP dot, indicating that some KT-MT interactions are resistant to nocodazole treatment or some kinetochores reestablish the interaction with microtubules after disconnection even in the presence of nocodazole.

To further verify that all GFP dots observed are clusters of functional kinetochores, we examined the localization of GFP-marked centromere on chromosome IV (*CEN4*-GFP) with mCherry-labeled Nuf2, another kinetochore protein. After G_1 cells were released into nocodazole for 120 min, we found that the *CEN4*-GFP dot colocalized with either the bigger or the smaller mCherry dot (Supplemental Figure S2), indicating that even the smaller fluorescent dots are real kinetochores. This result is in agreement with a previous observation that some kinetochores detach from the spindle microtubules after nocodazole treatment (Gillett *et al.*, 2004).

A smaller Mtw1-GFP focus in nocodazole-treated yeast cells could be a single kinetochore or a cluster. If the smaller kinetochore focus away from the spindle poles is from a single chromosome, we expect the fluorescence intensity of the larger foci to be 15 times larger than that of the smaller ones, as a haploid yeast cell contains 16 chromosomes. Therefore we analyzed the fluorescence intensity in cells that contain two GFP dots after nocodazole treatment and found that the average ratio is 2.25 ($n = 100$). Obviously, this ratio is much less than 15. Thus it is very likely that more than one kinetochore consists of the smaller kinetochore foci that are not linked to microtubules. In other words, kinetochores are clustered in the absence of KT-MT interaction.

Previous work showed that pericentric chromatin in budding yeast is organized into an intramolecular loop, and the loops from the 16 chromosomes form a cylindrical array. Although cohesin is not required for loop formation, it was proposed that cohesin may contribute to the stability or proximity of the intramolecular loops (Yeh *et al.*, 2008). To test whether cohesin facilitates kinetochore clustering, we examined kinetochore distribution in cohesin mutant cells (*scc1-73/mcd1*) that were released into 37°C nocodazole medium for 120 after G_1 arrest. We did not detect an obvious difference in the number of Mtw1-GFP foci per cell in WT and *scc1-73* mutant cells, suggesting that cohesin may not be directly involved in kinetochore clustering upon nocodazole treatment (Figure 1C). In addition, we failed to detect a dramatic kinetochore clustering defect in nocodazole-treated *GAL-SCC1* cells growing in glucose medium, which represses the expression of cohesin Scc1/Mcd1 (Supplemental Figure S3A). Furthermore, *ctf8*Δ, *ctf18*Δ, and *dcc1*Δ mutant cells were shown to have a cohesion defect (Mayer *et al.*, 2001), but they did not exhibit an obvious kinetochore clustering defect after nocodazole treatment (Supplemental Figure S3B).

Slk19 is required for kinetochore clustering after nocodazole treatment

Because kinetochores form clusters when they are away from spindle poles, kinetochore protein(s) is likely responsible for this clustering. Thus we analyzed kinetochore clustering in some yeast mutant cells lacking a nonessential kinetochore protein. For this purpose, we first constructed WT and *slk19*Δ kinetochore mutant strains in *MTW1-GFP TUB1-mCherry* background in order to visualize the kinetochore localization and the spindle structure. Like WT cells, *slk19*Δ mutant cells showed normal kinetochore clustering in an undisturbed cell cycle, with one GFP dot in G1 and S phase and two after metaphase (Supplemental Figure S4). After G_1-arrested cells were released into nocodazole for 120 min, most WT cells showed two or three Mtw1-GFP foci, whereas *slk19*Δ mutant cells exhibited an obvious clustering defect, as evidenced by the increased number of Mtw1-GFP foci per cell. We observed that 79.5% of *slk19*Δ cells showed more than three Mtw1-GFP foci, compared with only 6.0% for WT cells (Figure 2A). No spindle structure (Tub1-mCherry) was observed in both WT and *slk19*Δ mutant cells, indicating microtubule depolymerization under this condition. We further used super-resolution microscopy to examine the kinetochore distribution in nocodazole-treated cells, and it was obvious that *slk19*Δ cells exhibited an increased number of Mtw1-GFP foci (Figure 2A, middle). We noticed the presence of several low-intensity GFP foci in some *slk19*Δ mutant cells. Further experiments are needed to clarify whether the smaller foci represent single pairs of sister kinetochores. We also examined the kinetochore distribution in other nonessential kinetochore mutant cells. In contrast to *slk19*Δ, no obvious kinetochore clustering defect was observed in *ctf3*Δ and *ydr532c*Δ (*kre28*Δ) mutant cells (Supplemental Figure S5).

The difference in kinetochore clustering between WT and *slk19*Δ cells might be attributed to their differential microtubule-depolymerizing dynamics after nocodazole treatment, as previous data indicate the role of Slk19 in spindle stability during anaphase (Zeng *et al.*, 1999; Pereira and Schiebel, 2003). Therefore we trapped *TUB1-GFP* and *slk19*Δ *TUB1-GFP* cells in a chamber with flowed yeast extract/peptone/dextrose (YPD) medium. We used live-cell imaging to follow the Tub1-GFP signal after addition of nocodazole to the flowed medium (20 μg/ml). WT and *slk19*Δ mutant cells exhibited similar kinetics for the disappearance of spindle structure after nocodazole addition (Figure 2B), indicating that the kinetochore declustering in nocodazole-treated *slk19*Δ mutant cells is unlikely due to faster microtubule-depolymerizing kinetics. Unlike the *TUB1-mCherry* strains used in Figure 2A, we found that some yeast cells with Tub1-GFP showed a GFP dot after nocodazole treatment, which likely represents the short microtubules associated with the spindle pole body. We speculate that these residual microtubules may contribute to the clustering of kinetochores that colocalize with the spindle pole after nocodazole treatment, but the clustering of kinetochores away from the spindle pole in nocodazole-treated cells is likely independent of the microtubules that connect kinetochores to the spindle pole. However, we cannot exclude the possibility that Slk19 promotes kinetochore clustering through the interaction with kinetochore-derived microtubules (Ortiz *et al.*, 2009; Kitamura *et al.*, 2010).

As a kinetochore protein, Slk19 is also a component of FEAR, one of the mitotic exit pathways. To test the possibility that functional FEAR contributes to kinetochore clustering, we examined Mtw1-GFP distribution in cells lacking Spo12, which also functions in the FEAR pathway (Stegmeier *et al.*, 2002). In contrast to *slk19*Δ, most of *spo12*Δ mutant cells showed two or three kinetochore clusters after nocodazole treatment, like WT cells (Supplemental Figure S6). Therefore the kinetochore clustering defect in *slk19*Δ mutant is likely independent of its role in mitotic exit.

To further confirm the kinetochore clustering defect in *slk19*Δ mutant cells, we used a strain with two GFP-marked centromeres, *CEN4*-GFP and *CEN5*-GFP. Our rationale is that if Slk19 participates in kinetochore clustering, then we should observe a lower percentage of cells with colocalized *CEN4*-GFP and *CEN5*-GFP in *slk19*Δ mutant cells after nocodazole treatment compared with WT cells. After G_1-arrested cells were released into media containing nocodazole for 120 min, 35.6% of WT cells showed colocalization of *CEN4*-GFP and *CEN5*-GFP, whereas only 17.3% of *slk19*Δ cells did (Figure 2C). Thus the chance of colocalization of kinetochores from chromosome IV and V in *slk19*Δ cells is significantly lower than that in WT

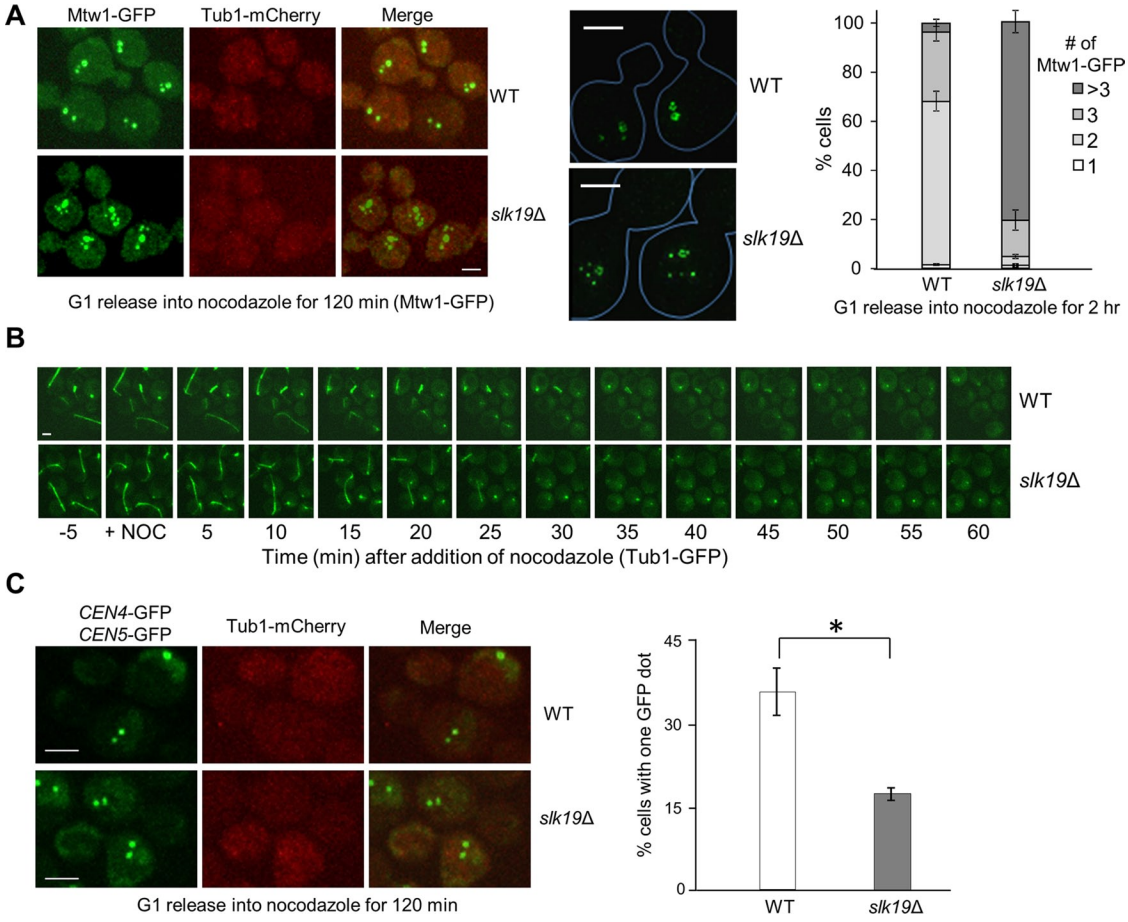

FIGURE 2: Slk19 is required for kinetochore clustering after nocodazole treatment. (A) *slk19*Δ mutants show a kinetochore clustering defect. G_1-arrested WT and *slk19*Δ cells in a *MTW1-GFP TUB1-mCherry* background were released into 20 µg/ml nocodazole for 120 min. After fixation, >100 cells were counted for the number of Mtw1-GFP foci per cell. Right, the average of three separate experiments. Left, representative images for Mtw1-GFP and Tub1-mCherry signals from confocal microscopy. Middle, representative images for Mtw1-GFP signals from superresolution microscopy. Bar, 3 µm. (B) *slk19*Δ mutant cells show similar microtubule-depolymerizing kinetics as WT cells. WT and *slk19*Δ cells with Tub1-GFP were loaded into a chamber where YPD medium containing 20 µg/ml nocodazole started to flow over the cells at time 0. Maximum-projection images were then created to show the spindle morphology over time. (C) Fewer *slk19*Δ cells show colocalized centromeres from chromosomes IV and V after nocodazole treatment. WT and *slk19*Δ cells in a *TUB1-mCherry* background with GFP-marked centromeres of chromosome IV and V (*CEN4-GFP CEN5-GFP*) were grown to log phase at 25°C. After G_1 arrest, the cells were released into 20 µg/ml nocodazole for 120 min and then harvested and fixed for fluorescence microscopy. The number of GFP dots per cell was counted in >100 cells, and the average from triplicates is shown. Confocal microscopy was used to project representative maximum-intensity images for *CEN4-GFP*, *CEN5-GFP*, and Tub1-mCherry. Bar, 3 µm.

cells, confirming that Slk19 is required to cluster kinetochores from separated chromosomes in the presence of nocodazole.

*slk19*Δ mutant cells exhibit a delay in the reestablishment of the KT-MT interaction

Our data suggest that Slk19 functions as a glue to mediate the interaction of kinetochores from separate chromosomes. We next asked how Slk19's kinetochore function facilitates chromosome segregation. Previous data indicate that *slk19*Δ mutant cells exhibit normal chromosome segregation kinetics (Sullivan *et al.*, 2001; Jin *et al.*, 2008), but the synthetic lethality between *slk19*Δ and spindle assembly checkpoint mutants suggests a role of Slk19 in faithful chromosome segregation. Therefore we first assessed the sensitivity of *slk19*Δ mutants to the microtubule poison benomyl. Although *slk19*Δ cells grew normally on YPD plates, a rich medium for yeast cells, the mutant cells showed a clear slow-growth phenotype on plates containing 15 µg/ml benomyl (Figure 3A). In contrast, *spo12*Δ cells did not show any noticeable benomyl sensitivity, suggesting that the slow-growth phenotype of *slk19*Δ mutants is not due to the defect in mitotic exit. Therefore the kinetochore function of Slk19 might become essential when cells are challenged with microtubule-depolymerizing agents.

Defects in KT-MT interaction trigger the spindle assembly checkpoint to delay the cell cycle through the stabilization of the anaphase inhibitor Pds1 (Cohen-Fix *et al.*, 1996). In the absence of nocodazole treatment, *slk19*Δ cells exhibited only a slight delay in Pds1 degradation (Figure 4B), which is in agreement with previous data (Sullivan *et al.*, 2001). Next we released the G_1-arrested WT and *slk19*Δ mutant cells into 20 µg/ml nocodazole for 120 min and then washed off the nocodazole to monitor the cell cycle response to nocodazole treatment. In the presence of nocodazole, *slk19*Δ budded normally, similar to WT cells. After nocodazole washout,

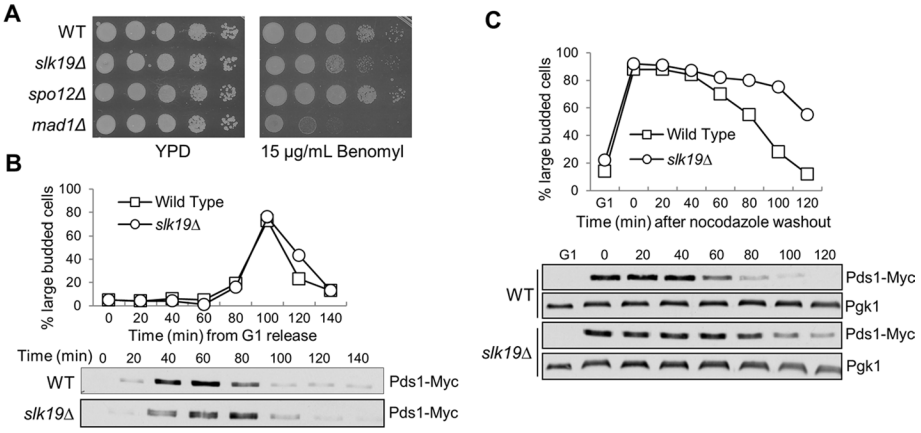

FIGURE 3: *slk19* mutant cells show delayed anaphase entry after nocodazole treatment. (A) *slk19*Δ mutants show sensitivity to benomyl. WT, *slk19*Δ, *spo12*Δ, and *mad1*Δ mutant cells were grown to saturation, 10-fold diluted, and spotted onto YPD with and without 15 μg/ml benomyl. The plates were scanned after incubation at 30°C for 3 d. (B) *slk19*Δ mutants do not show an obvious cell cycle defect in an unperturbed cell cycle. WT and *slk19*Δ cells with *PDS1-18myc* were released from G_1 into YPD at 25°C. Cells were harvested every 20 min and examined for their budding index and Pds1 protein levels. (C) *slk19*Δ mutants show an anaphase entry delay after exposure to nocodazole. G_1-arrested WT and *slk19*Δ cells with *PDS1-18myc* were released into YPD containing 20 μg/ml nocodazole at 25°C for 120 min. Nocodazole was then washed off, and the cells were released into YPD medium at 25°C. Cells were harvested every 20 min for budding index and Pds1 protein levels. Pgk1 protein level is shown as a loading control.

however, *slk19*Δ cells showed an obvious delay in the transition from large-budded to unbudded cells. Consistent with the budding index, *slk19*Δ cells also showed stabilized Pds1 protein after nocodazole exposure (Figure 3C). Because the disappearance of Pds1 protein marks anaphase entry (Cohen-Fix *et al.*, 1996), this result suggests that *slk19*Δ cells may have difficulty in establishing correct KT-MT interaction after nocodazole treatment. Previous work indicates that *slk19*Δ mutant cells lose viability quickly after treatment with nocodazole (Pfiz *et al.*, 2002), but we did not observe significant viability loss with our *slk19*Δ strains, which could be attributed to different genetic backgrounds.

Our data suggest that Slk19 protein keeps kinetochores together after their disconnection from the spindle poles. To reestablish the KT-MT interaction, the disconnected kinetochores are first captured by a microtubule and then moved to the vicinity of one spindle pole through Cik1/Kar3-mediated transport (Tanaka *et al.*, 2005, 2007), which may facilitate chromosome bipolar attachment (Liu *et al.*, 2011). Clustered kinetochores might be transported to a spindle pole as a group, thereby facilitating the reestablishment of KT-MT interaction. To test this idea, we compared the kinetochore capture process in WT and *slk19*Δ cells after nocodazole treatment. The G_1-arrested cells were released into nocodazole medium for 100 min to disrupt KT-MT interaction. After nocodazole was washed off, the cells were subjected to live-cell microscopy, and the colocalization of kinetochore (Mtw1-GFP) and spindle (Tub1-mCherry) was examined. Note that spindle reformation varied slightly from cell to cell, but the average time was similar between WT and *slk19*Δ cells. As described earlier, most WT cells showed two or three Mtw1-GFP foci just after the release from nocodazole, but *slk19*Δ mutant cells exhibited more GFP foci. The kinetochore capture process in representative WT and *slk19*Δ cells is shown in Figure 4A. In the WT cell, the mCherry cluster appeared 24 min after the movie was started, and all Mtw1-GFP signals colocalized with Tub1-mCherry at 30 min. Thus this cell finished the kinetochore capture within 6 min. In contrast, the visible Tub1-mCherry cluster appeared at 30 min in the *slk19*Δ cell, but the complete colocalization of all the GFP-marked kinetochores and mCherry-labeled spindle occurred at 48 min, showing that this cell needs 18 min to achieve kinetochore capture. On average, it took WT cells 16 min for all the GFP foci to colocalize with the spindle after nocodazole washout. It is striking that *slk19*Δ mutant cells took an average of 40 min to achieve the colocalization (n = 70). We noticed that four *slk19*Δ cells failed to achieve complete colocalization during the entire course of the experiment (150 min), and these cells were excluded for the calculation of the average capture time. Furthermore, we found that many of the cells formed a single GFP dot at first, and then two separated foci appeared before spindle elongation, presumably indicating the time window between chromosome capture and the establishment of chromosome bipolar attachment.

Using the same approach, we also compared the capture process for a single kinetochore in WT and *slk19*Δ cells with *CEN4-GFP* and *TUB1-mCherry*. Consistently, *slk19*Δ cells showed an obvious delay in the colocalization of *CEN4*-GFP with the spindle compared with WT cells (Figure 4B), but the delay was not as dramatic as that from the strains with Mtw1-GFP. We speculate that this difference is due to the fact that *CEN4*-GFP represents one of the 16 pairs of sister kinetochores. Taken together, these results suggest that Slk19-dependent kinetochore clustering facilitates chromosome capture after the disruption of the KT-MT interaction.

*slk19*Δ mutant cells exhibit delayed chromosome bipolar attachment after exposure to nocodazole

The live-cell microscopy data indicate that *slk19*Δ cells show a delay in kinetochore capture after nocodazole treatment, but the delay in anaphase onset in *slk19*Δ cells as indicated by spindle elongation is more dramatic (Figure 4A). It is possible that Slk19 also plays a role in chromosome bipolar attachment in addition to the kinetochore capturing. To test this idea, we first grew *cdc13-1* and *cdc13-1 slk19*Δ cells at 34°C to achieve preanaphase arrest, as loss of Cdc13 function creates unprotected telomeres that activate the DNA-damage checkpoint (Lin and Zakian, 1996). We then treated the cells with nocodazole. The nocodazole treatment of *cdc13-1*–arrested cells did not cause kinetochore declustering, and that was also true for *cdc13-1 slk19*Δ cells. After nocodazole was washed off, we examined the localization of *CEN4*-GFP relative to the spindle over time while keeping the cells at 34°C to retain the preanaphase arrest. The localization of a single or separated GFP dots at the center region of the spindle indicates bipolar attachment on chromosome IV. We counted cells containing a *CEN4*-GFP dot within the center region of a spindle (one-third) in this category (Figure 5A, arrow), whereas the localization of a *CEN4*-GFP dot at the end of a spindle suggests failed bipolar attachment. Just after nocodazole release, no spindle structure appeared in both *cdc13-1* and *cdc13-1 slk19*Δ cells. After release from nocodazole treatment for 30 min, 56.8% of *cdc13-1* cells exhibited *CEN4*-GFP localization at the center region of the spindle, whereas

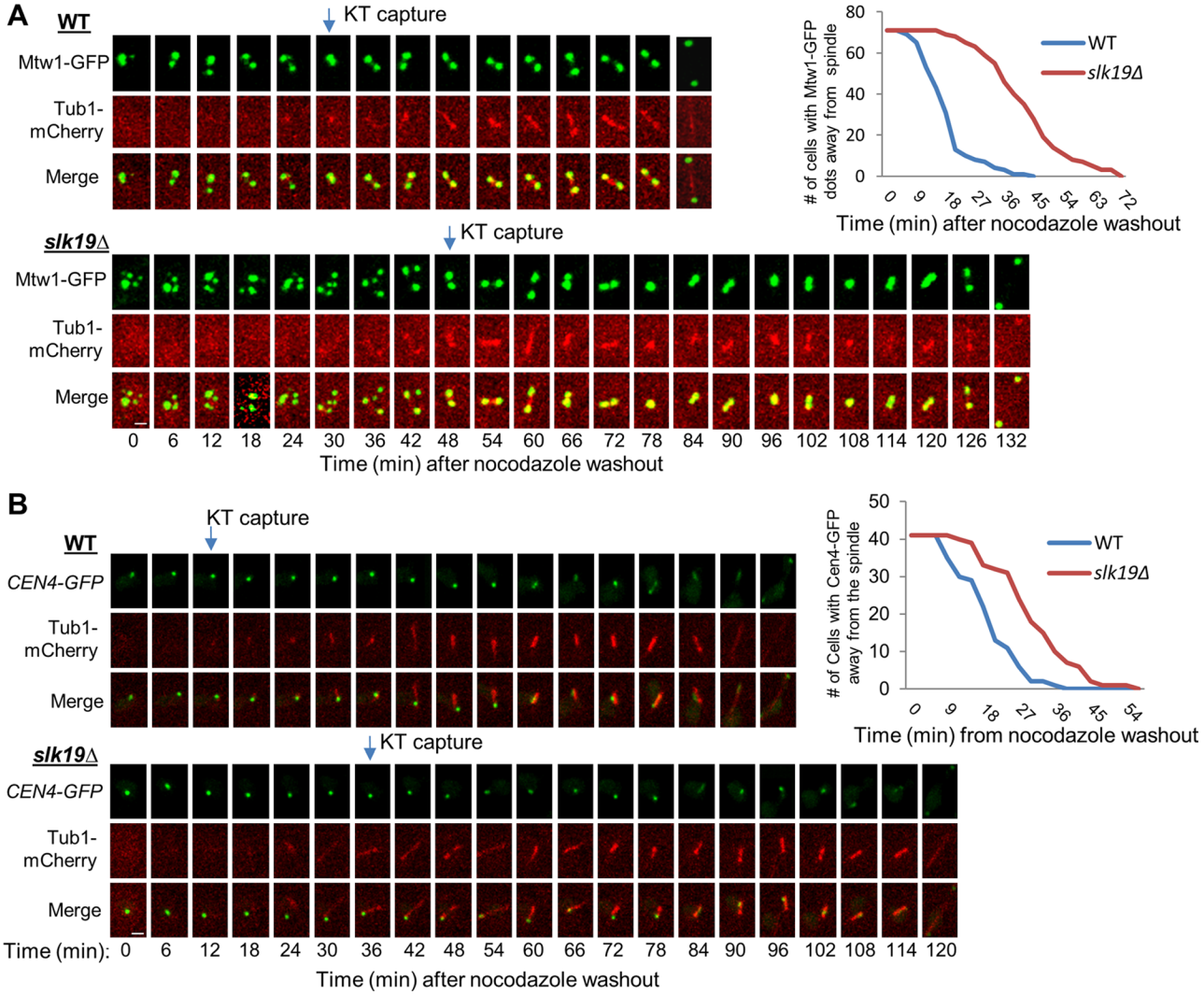

FIGURE 4: *slk19*Δ mutant cells show kinetochore capture defect after nocodazole treatment. (A) *slk19*Δ mutant cells show a dramatic delay in kinetochore capture after the disruption of KT-MT interaction by nocodazole. G_1-arrested WT and *slk19*Δ cells with *MTW1-GFP TUB1-mCherry* were released into YPD containing 20 μg/ml nocodazole for 100 min. After nocodazole was washed off, the cells were transferred onto an agarose pad on a microscope slide to perform live-cell imaging at 25°C. Although it took 8 min to prepare the slide and start the live-cell imaging after nocodazole washout, we set the movie starting point as time 0 for convenience. The localization of Mtw1-GFP and the spindle structure over the time course in a representative cell of WT and *slk19*Δ are shown. The timing of kinetochore capture was assessed based on the movies made from the live-cell imaging, and we define the point of kinetochore capture as when all Mtw1-GFP signals colocalize with the spindle (Tub1-mCherry). Right, kinetochore-capture kinetics in the WT and *slk19*Δ cells ($n = 70$). Scale bar, 3 μm. (B) *slk19*Δ mutant cells exhibit delayed capture of a GFP marked chromosome IV (*CEN4*-GFP) by spindle microtubule. WT and *slk19*Δ cells with *CEN4-GFP TUB1-mCherry* were treated the same as in A. The point when the *CEN4*-GFP colocalizes with the spindle was defined as kinetochore capture. Left, localization of *CEN4*-GFP and spindle morphology in representative WT and *slk19*Δ cells over time. Right, kinetics of kinetochore capture for chromosome IV in WT and *slk19*Δ mutant cells ($n = 41$). Scale bar, 3 μm.

only 27.9% of *cdc13-1 slk19*Δ cells showed this phenotype. *cdc13-1 slk19*Δ cells also showed a lower percentage of cells with the *CEN4*-GFP dot at the spindle center after nocodazole release for 45 and 60 min, and thus *slk19*Δ mutant cells appeared to take longer time to achieve bipolar attachment (Figure 5A). These results suggest that *slk19*Δ mutants may display a chromosome bipolar attachment defect after nocodazole treatment. Because treatment of *cdc13-1 slk19*Δ cells growing at 34°C did not cause defective kinetochore clustering, the delayed bipolar attachment in *slk19*Δ cells is likely independent of the kinetochore capture defect.

The delay of chromosome bipolar attachment in *slk19*Δ cells could increase the chance of syntelic attachments, in which both sister kinetochores are connected to microtubules emanating from a single spindle pole. Sgo1 is a component of the tension checkpoint that senses syntelic attachment and delays anaphase onset (Indjeian *et al.*, 2005; Jin *et al.*, 2012). If syntelic attachments occur in *slk19*Δ cells after nocodazole treatment, these cells will show a Sgo1-dependent cell cycle delay. Because *sgo1*Δ cells are sensitive to nocodazole treatment in G_1 phase but are insensitive when first arrested at G_2/M phase (Indjeian and Murray, 2007), we generated *slk19*Δ, *sgo1*Δ, and *slk19*Δ *sgo1*Δ strains in *cdc13-1 CEN4-GFP*

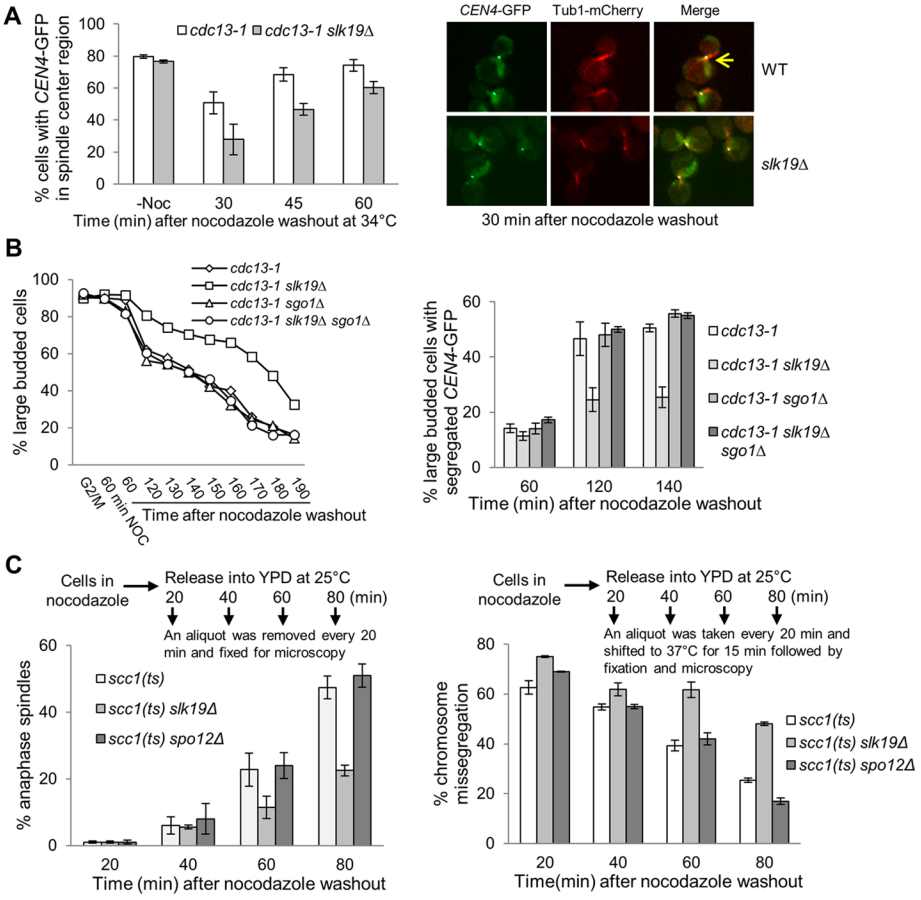

FIGURE 5: *slk19*Δ mutant cells show capture-independent defect in chromosome bipolar attachment. (A) *slk19*Δ mutants show a lower percentage of cells with the *CEN4*-GFP in the middle of the spindle after nocodazole treatment of cells arrested in preanaphase. *cdc13-1* and *cdc13-1 slk19*Δ cells with *CEN4-GFP TUB1-mCherry* were first incubated in 34°C medium to achieve preanaphase arrest. Then we added 20 μg/ml nocodazole into the medium for 60 min to disrupt the spindle structure. After nocodazole was washed off, the cells were released into 34°C YPD medium, and the relative localization of *CEN4*-GFP to the spindle was assessed over time. We counted the percentage of cells with the *CEN4*-GFP dot within the one-third of the center region of the spindle, and at least 100 cells were counted for each sample. The average from three independent experiments is shown. Right, representative images. (B) *slk19*Δ mutants show tension checkpoint–dependent anaphase entry delay after nocodazole exposure. G_1-arrested WT, *slk19*Δ, *sgo1*Δ, and *slk19*Δ *sgo1*Δ in a *cdc13-1 CEN4-GFP* background were released to 34°C YPD medium for 120 min to achieve preanaphase arrest. The cells were then shifted to a medium containing 20 μg/ml nocodazole and incubated at 25°C for 60 min. After nocodazole was washed off, the cells were resuspended in fresh YPD media at 25°C and harvested over time to examine budding index and *CEN4*-GFP segregation. More than 100 cells were counted for each sample. Left, percentage of large-budded cells. Right, percentage of cells with segregated *CEN4*-GFP dots (one GFP dot in each mother and daughter cell) at the indicated time points. (C) *slk19*Δ mutant cells exhibit more chromosome missegregation after nocodazole exposure in a cohesin mutant. G_1-arrested *scc1-73, scc1-73 slk19*Δ, and *scc1-73 spo12*Δ cells with *CEN5-GFP TUB1-mCherry* were released into YPD containing 20 μg/ml nocodazole for 120 min at 25°C. After nocodazole washout, cells were released into 25°C YPD medium and removed every 20 min to examine the spindle structure. In parallel, an aliquot of the cells was taken every 20 min and shifted to 37°C for 15 min to inactivate cohesin. After fixation, we examined the localization of *CEN5*-GFP only in cells with an anaphase spindle, and the presence of one or two GFP dots within a single cell body indicates *CEN5*-GFP missegregation. Left, average percentage of cells with anaphase spindle. Right, average percentage of cells with cosegregated *CEN5*-GFP after the shift to 37°C. More than 100 cells were counted for each sample, and the average is from three separate experiments.

background. After achieving G_2/M arrest by growing the cells at 34°C, we shifted the cells to 25°C medium containing 20 μg/ml nocodazole. After incubation for 60 min, we washed off nocodazole and released the cells into YPD medium at 25°C to follow the cell cycle progression. Compared to *cdc13-1* single mutant, more *cdc13-1 slk19*Δ cells remained as large budded. Of interest, the delayed M-to-G_1 transition in *cdc13-1 slk19*Δ mutants was completely suppressed by *sgo1*Δ. Moreover, *cdc13-1 slk19*Δ cells exhibited a significant delay in segregation *CEN4*-GFP, and this delay was also suppressed by *sgo1*Δ (Figure 5B). Consistently, *cdc13-1 slk19*Δ *sgo1*Δ double mutants exhibited increased viability loss after nocodazole treatment (unpublished data). Given the established checkpoint function of Sgo1 in sensing syntelic attachments, we speculate that the loss of function of Slk19 delays the establishment of chromosome bipolar attachment after nocodazole treatment and increases the frequency of syntelic attachment.

Faulty KT-MT attachment activates the spindle checkpoint to prevent spindle elongation. In cells lacking sister chromatid cohesion, however, the spindle will elongate even in the presence of these faulty attachments, which will allow us to visualize chromosome missegregation. Thus we created *scc1-73 (mcd1), scc1-73 slk19*Δ, and *scc1-73 spo12*Δ strains in *CEN5-GFP TUB1-mCherry* background, which will lose cohesion when incubated at 37°C (Michaelis *et al.*, 1997). Cells arrested in G_1 phase were released into nocodazole for 120 min at 25°C to disrupt the spindle structure. After nocodazole washout, the cells were released into 25°C YPD to examine the spindle morphology over time. At 80 min after nocodazole washout, 47.4% of WT cells, but only 22.5% of *slk19*Δ cells, showed an elongated spindle, indicating an anaphase entry delay in *slk19*Δ mutants. In contrast, *spo12*Δ mutant cells did not show any delay in spindle elongation compared with WT cells (Figure 5C, left). Thus *slk19*Δ mutant cells showed delayed metaphase–anaphase transition after nocodazole exposure.

In parallel, a portion of the cells was removed every 20 min after nocodazole washout and shifted to 37°C for 15 min to inactivate cohesin (see the diagram in Figure 5C for an illustration of the experiment). After fixation, *CEN5*-GFP segregation was only scored in cells with an elongated spindle. The rationale for this experiment is that the abolition of cohesion will allow spindle elongation regardless of proper chromosome attachment. If *slk19*Δ cells take longer to form bipolar attachment after nocodazole washout, then these cells will be more prone to chromosome missegregation after cohesin inactivation. After nocodazole washout for 20 and 40 min, the temperature shift caused a high frequency of *CEN5*-GFP cosegregation in all three strains,

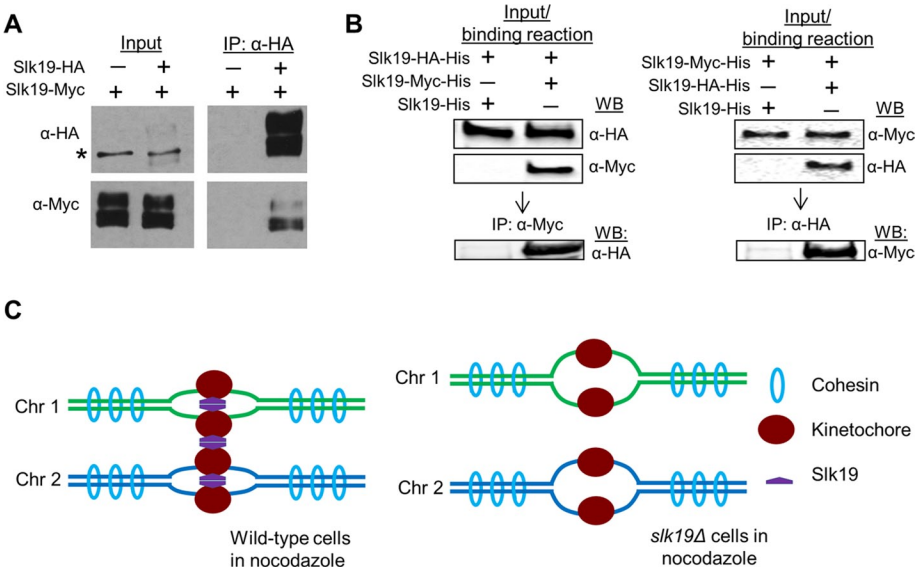

FIGURE 6: Slk19 protein forms dimers. (A) Both full-length and cleaved fragment of Slk19 physically interact with themselves. Diploid yeast strains containing either *SLK19/SLK19-13Myc* or *SLK19-6HA/SLK19-13Myc* were grown to log phase. The cells were harvested to prepare the whole cell extracts with a bead beater. The extracts were first incubated with anti-HA antibody, and then protein A/G-coated agarose beads were added. Western blotting was performed to detect Slk19-6HA and Slk19-13Myc in the whole-cell extracts and the immunoprecipitates. Asterisk indicates a nonspecific band. (B) Slk19 interacts with itself in vitro. Purified Slk19-HA-His was mixed with Slk19-His or Slk19-Myc-His, and then the mixtures were pulled down with anti-Myc antibody. Slk19 proteins with different tags in the mixture and immunoprecipitates were detected using Western blotting with anti-Myc and anti-HA antibodies. A similar pull-down assay was performed after the mixture of Slk19-Myc-His with Slk19-His or Slk19-HA-His. (C) The working model for Slk19-dependent kinetochore clustering and sister kinetochore cohesion.

indicating the failure of chromosome attachment. After nocodazole release for 80 min, however, the difference in the frequency of *CEN5*-GFP missegregation between WT, *spo12*Δ, and *slk19*Δ mutant cells became very significant (25.4% for WT vs. 48.1% for *slk19*Δ; Figure 5C, right), indicating that Slk19 is required for the efficient establishment of chromosome bipolar attachment after nocodazole exposure. Given that our data indicate that most of WT and *slk19*Δ mutant cells can finish chromosome capture 80 min after nocodazole washout (Figure 4A), we speculate that Slk19 also promotes bipolar attachment in addition to its role in chromosome capture. Because *spo12*Δ mutant cells did not show any defect in chromosome bipolar attachment after nocodazole exposure, we conclude that the kinetochore function of Slk19 is independent of its role in mitotic exit.

Dimerization of Slk19 might be required for its kinetochore function

Slk19 is a protein with seven coiled-coil motifs that localize in its central region and C-terminus (Zeng *et al.*, 1999; Zhang *et al.*, 2006). The coiled-coil motifs are made up of α-helices that usually mediate protein dimerization (Lupas and Gruber, 2005). Indeed, genome-wide studies indicate that Slk19 can interact with itself (Newman *et al.*, 2000; De Wulf *et al.*, 2003; Wong *et al.*, 2007; Tarassov *et al.*, 2008). To confirm the Slk19–Slk19 interaction, we generated a *SLK19-HA/SLK19-Myc* diploid strain. Anti-hemagglutinin (HA) antibody was used to immunoprecipitate the cell lysate from cycling cells, and then proteins were probed with anti-Myc and anti-HA antibodies after separation. In the immunoprecipitate, we detected both full-length and fragments of Slk19-Myc (Figure 6A). The short forms of Slk19 are likely cleavage products, based on previous studies (Sullivan *et al.*, 2001). The coimmunoprecipitation result indicates the Slk19–Slk19 interaction and Slk19 cleavage do not regulate this interaction.

To further test whether Slk19 directly interacts with itself in vitro, we purified Slk19-histidine (His), Slk19-HA-His, and Slk19-Myc-His from bacterial lysates (Supplemental Figure S7). We first mixed purified Slk19-HA-His proteins with either Slk19-His or Slk19-Myc-His. We then used anti-Myc to immunoprecipitate the mixtures and performed Western blotting by probing with anti-Myc and anti-HA antibodies. We detected a strong Slk19-HA-His band from both mixtures; however, only the mixture containing Slk19-Myc-His and Slk19-HA-His showed an anti-HA band after immunoprecipitation with anti-Myc antibody (Figure 6B, left). Similarly, anti-HA antibody could also pull down Slk19-Myc-His in the mixture containing Slk19-HA-His and Slk19-Myc-His (Figure 6B, right). Together these in vivo and in vitro results demonstrate that Slk19 directly interacts with itself. We speculate that Slk19 dimerization leads to the formation of bridges between kinetochores (Figure 6C).

DISCUSSION

The kinetochore clustering in budding yeast has been documented for many years, but the biological significance of this clustering has remained a mystery. Moreover, it is unclear whether this clustering is totally dependent upon the KT-MT interaction. Here we report that the kinetochore protein Slk19 clusters kinetochores, which is likely independent of KT-MT interaction. We further show that, in the absence of Slk19, kinetochore capture and the establishment of chromosome bipolar attachment are delayed after the disruption of the KT-MT interaction by nocodazole. We also show in vivo and in vitro evidence indicating that Slk19 protein interacts with itself. Therefore we propose a model in which Slk19–Slk19 interaction leads to kinetochore clustering (Figure 6C), a mechanism that becomes critical for chromosome capture and bipolar attachment after the disruption of KT-MT interaction.

Our data indicate that the Slk19-mediated kinetochore clustering is likely independent of the microtubules that connect kinetochores to the spindle poles. First, the scattered kinetochores in nocodazole-treated *slk19*Δ mutant cells are away from the spindle pole, suggesting the loss of connection with the spindle poles. Moreover, the *slk19*Δ mutant cells show similar microtubule depolymerizing kinetics as WT cells in response to nocodazole treatment (Figure 2B). In addition to spindle poles, recent data indicate that kinetochores also generate microtubules (Ortiz *et al.*, 2009; Kitamura *et al.*, 2010). Thus it is possible that Slk19 promotes kinetochore clustering by associating and/or stabilizing these microtubules. Another possibility is that Slk19 binds to other kinetochore proteins directly, and the Slk19–Slk19 interaction leads to kinetochore clustering.

Previous work showed abnormal nuclear morphology in *slk19*Δ mutant cells (Zhang *et al.*, 2006). One interesting question is whether the kinetochore clustering defect is secondary to the abnormal

chromatin structure. Because nocodazole treatment abolishes the abnormal nuclear morphology seen in *slk19*Δ cells (Zhang *et al.*, 2006), the kinetochore declustering in nocodazole-treated *slk19*Δ cells is unlikely a consequence of the abnormal nuclear morphology. Instead, the enriched localization of Slk19 at kinetochores suggests that the kinetochore function of Slk19 likely contributes to kinetochore clustering. In addition, the data from the Dawson lab show the colocalization of Slk19 with another kinetochore protein, Mtw1 (Havens *et al.*, 2010). We also performed live-cell imaging in cells with *SLK19-GFP NUF2-mCherry* and found the colocalized Slk19 and kinetochore protein Nuf2 until anaphase, when the spindle midzone localization of Slk19 was noticed (unpublished data). Because we showed direct Slk19–Slk19 interaction, one possibility is that the interaction between Slk19 proteins from different kinetochores mediates kinetochore clustering (Figure 6C), but more experiments are needed to confirm this model.

In nocodazole-treated *slk19*Δ mutant cells, in addition to a major kinetochore cluster that associated with the spindle poles, more small Mtw1-GFP foci were detected. One interesting question is whether the smaller Mtw1-GFP dot represents a single pair of sister kinetochores. In some *slk19*Δ cells, we observed as many as nine Mtw1-GFP foci. Given that yeast cells have only 16 pairs of sister chromatids in G_2/M phase, some of the smaller foci have to be a single pair of sister kinetochores. In nocodazole-treated *slk19*Δ cells, some kinetochores may stay together even when they are disconnected from the spindle pole. One possibility is that these kinetochores just colocalize by chance but without any linkage. Alternatively, an unknown mechanism clusters these kinetochores in the absence of Slk19 and KT-MT interaction. Therefore further analysis is necessary to determine whether kinetochore clustering is abolished completely in *slk19*Δ mutant cells once they become disconnected from the spindle pole.

Kinetochore declustering was also observed in other kinetochore mutants, such as *nuf2-60* and *ndc80-1*, even without treatment with nocodazole (Janke *et al.*, 2001; Anderson *et al.*, 2009). Nuf2 and Ndc80 are components of the Ndc80 kinetochore complex, which is required for the KT-MT interaction. Recent data show that the association of Slk19 with kinetochore is abolished in some temperature-sensitive kinetochore mutant strains when incubated at 37°C, including *spc105^{ts}*, *ndc80-1*, and *mtw1-1* (Pagliuca *et al.*, 2009). Therefore it is possible that the abolished KT-MT interaction alone causes kinetochore clustering. Alternatively, both the loss of the KT-MT interaction and the absence of Slk19 at kinetochores are necessary for kinetochore declustering.

What is the biological significance of this Slk19-dependent kinetochore clustering? For the kinetochores that lose their connection to the spindle pole, the highly dynamic spindle microtubules are responsible for their capture. Then the minus end–directed motor complex Cik1/Kar3 transports the captured kinetochores toward the vicinity of the spindle pole (Tanaka *et al.*, 2005). The increased distance between a kinetochore and the spindle pole will significantly reduce the chance of kinetochore capture. A whole kinetochore cluster will be moved to the spindle pole once only one kinetochore in this cluster is captured. This mechanism is expected to increase the efficiency for the transport of detached kinetochores toward the vicinity of a spindle pole, where they have a much higher chance to be captured by spindle microtubules. In support of this speculation, we observed a dramatic kinetochore capturing delay in *slk19*Δ mutant cells after the disruption of KT-MT interaction. Therefore kinetochore clustering could be an unidentified mechanism that facilitates kinetochore capture.

In budding yeast, an interesting observation is that sister kinetochores separate before anaphase entry (Goshima and Yanagida, 2000; He *et al.*, 2000). Because separase is inactive before anaphase onset, cohesin cleavage is unlikely the cause for this sister centromere separation. Work from the Bloom lab showed a cruciform structure of the pericentric chromatin (Yeh *et al.*, 2008). This observation indicates that the enriched cohesin at the pericentric region unlikely links sister centromeres, and instead it might stabilize the cruciform structure by introducing cohesion within a single chromatin at pericentric regions. Thus a unique mechanism may contribute to sister chromatid cohesion at centromeric regions. Our evidence suggests that Slk19 mediates interaction between kinetochores from different chromosomes. It is possible that Slk19 also mediates interaction between sister kinetochores, which contributes to sister-chromatid cohesion at centromeric regions. To test this possibility, we looped out a pair of GFP-marked centromeres of chromosome IV in nocodazole-treated cells and found that *slk19*Δ cells showed higher frequency of separated sister centromeres (Supplemental Figure S8). However, the result could not support a solid conclusion because of the lower frequency of the excision of the centromere from chromosome IV, as indicated by only 40% viability loss after the induction of recombination. If the Slk19–Slk19 interaction contributes to sister kinetochore cohesion, the tension resulting from chromosome bipolar attachment can separate sister kinetochores and centromeres by breaking up the Slk19-Slk19 interaction in the absence of separase-dependent cohesin cleavage. Moreover, this Slk19-mediated sister centromere cohesion should be reversible. Indeed, separated sister centromeres in metaphase cells reunite after nocodazole treatment, and this reunion depends on Slk19 (Zhang *et al.*, 2006). Therefore both kinetochore clustering and sister chromatid cohesion at centromere regions could be attributed to Slk19-mediated interkinetochore interaction (Figure 6C).

Our data also indicate the role of Slk19 in the establishment of chromosome bipolar attachment. The exposure of *cdc13-1 slk19*Δ cells to nocodazole delayed the chromosome bipolar attachment significantly after nocodazole was washed off, and this delay depends on a functional tension checkpoint, indicating the presence of syntelic attachments. Because we did not observe obvious kinetochore declustering in these cells, it is likely that Slk19 also facilitates chromosome bipolar attachment in a kinetochore-clustering–independent manner. One explanation is that the Slk19–Slk19 interaction between sister kinetochores ensures their opposite orientation, which facilitates the bipolar attachment. In the absence of Slk19, however, the presence of misorientated sister kinetochores increases the frequency of syntelic attachment, especially after the disruption of KT-MT interaction.

Kinetochore clustering is also observed in higher eukaryotes (Solovei *et al.*, 2004), indicating that this mechanism could be conserved. Although a Slk19 homologue is lacking in higher organisms based upon protein sequence homology, several functional orthologues have been suggested due to its diverse functions (Sato *et al.*, 2003; Vos *et al.*, 2006; Ohkuni *et al.*, 2008). One of the candidates is the mammalian protein CENP-F/mitosin, which localizes to the kinetochore from late G_2 to early anaphase but moves to spindle midzone in late anaphase, a pattern similar to that of Slk19 (Rattner *et al.*, 1993; Liao *et al.*, 1995; Zhu *et al.*, 1995; Yang *et al.*, 2003). Of interest, knockdown of CENP-F leads to weakened centromeric-specific cohesion (Holt *et al.*, 2005). Moreover, more-scattered chromosome distribution in CENP-F knockdown cells is consistent with the function of CENP-F in kinetochore clustering, although further experiments are needed to confirm this notion (Holt *et al.*, 2005). Similar to Slk19, CENP-F has also been shown to dimerize (Zhu

et al., 1995). These similarities suggest that CENP-F could be the functional orthologue of yeast Slk19 in mammalian cells.

MATERIALS AND METHODS

Yeast strains and growth

The yeast strains used in this study are listed in Supplemental Table S1. All strains are isogenic to Y300, a W303 derivative. Yeast cells were grown in YPD or indicated synthetic medium. To arrest cells in G_1 phase, 5 μg/ml α-factor was added into cell cultures. After 120 min of incubation, the G_1-arrested cells were washed twice with water and then released into fresh medium to start cell cycle. Nocodazole was used at 20 μg/ml in 1% dimethyl sulfoxide. To induce the expression of *SCC1 (MCD1)* from a galactose-inducible promoter control, we first grew cells in raffinose medium and then added galactose to the medium to a final concentration of 2%.

Cytological techniques

Cells with GFP-, mApple-, or mCherry-tagged proteins were fixed with 3.7% formaldehyde for 5 min at room temperature, and then washed twice with 1× phosphate-buffered saline (PBS) buffer and resuspended in PBS buffer for fluorescence microscopy (Carl Zeiss MicroImaging, Jena, Germany). Live-cell microscopy was carried out with an Andor Revolution SD imaging system that uses a Nikon Eclipse Ti microscope (Andor Technology, South Windsor, CT). Glass depression slides were used to prepare an agarose pad filled with synthetic or complete medium. All live-cell images were acquired at 25°C with a 100× objective lens. Twelve *Z*-sections were collected at each time point, and each optical section was set at 0.5 μm thickness. The time-lapse interval was set at 3 or 5 min as indicated. Maximum projections from applicable time points were created using Andor IQ2 software. To visualize microtubule-depolymerizing dynamics, filtered YPD medium containing 20 μg/ml nocodazole was flowed over cells with Tub1-GFP trapped in a chamber (CellASIC, Hayward, CA). Superresolution images were taken from the DeltaVision OMX system from Applied Precision (Issaquah, WA). The error bars in all the figures represent the SEM.

Protein techniques

Cell pellets from 1.5 ml of cell culture were resuspended in 200 μl of 0.1 N NaOH and incubated at room temperature for 5 min. After centrifugation, the cells were resuspended in equal volume (30 μl) of double-distilled H_2O and SDS protein-loading buffer. The samples were then boiled for 5 min and resolved with 10% SDS-polyacrylamide gel. Proteins were detected with enhanced chemiluminescence (PerkinElmer LAS, Waltham, MA) after probing with anti-Myc antibody (Covance Research Products, Berkeley, CA) and horseradish peroxidase–conjugated secondary antibody (Jackson ImmunoResearch Laboratories, West Grove, PA).

Construction of slk19 bacterial-expression plasmids

To construct bacterial expression plasmids, we cloned the Slk19 open reading frame from yeast genomic DNA using PCR. The primers contain cut sites for the *Nde*I and *Not*I restriction enzymes. After PCR, the amplified product was digested with *Nde*I and *Not*I enzymes (New England BioLabs, Ipswich, MA) and ligated into the *NdeI*/*Not*I cloning site of the bacterial expression plasmid pET-20b(+) (Invitrogen, Carlsbad, CA) in frame with a C-terminal His tag. The cloned Slk19 was fully sequenced to make sure that no mutations were introduced during the cloning procedure. The resulting plasmid is referred to as pET-Slk19-His. To construct pET-Slk19-HA-His and pET-Slk19-Myc-His expression plasmids, we subcloned a double-stranded DNA oligonucleotide containing the coding sequence for HA or Myc tag (with *Not*I overhangs) into the *Not*I restriction site of the pET-Slk19-His plasmid. This results in an HA or Myc tag at the C-terminus of Slk19, in frame with the His tag. The correct frame and sequence of the tags were confirmed by sequencing.

Bacterial expression and purification of slk19 proteins

Slk19 plasmids were transformed into Rosetta (DE3) cells and grown in LB Miller broth medium (EMD Chemicals, San Diego, CA) with ampicillin (100 μg/ml final concentration) overnight at 37°C. The overnight bacterial culture was diluted 1:6 in LB–ampicillin and grown for 1 h at 37°C, then for 6 h at room temperature to allow for optimal expression of the Slk19 proteins. Bacterial cells were then pelleted by centrifugation and resuspended in ice-cold PBS, pH 7.5, supplemented with a cocktail of protease inhibitors (Sigma-Aldrich, St. Louis, MO). The suspension was sonicated on ice (three bursts, 15 s each, with 2-min intervals between sonication bursts to allow cooling). Bacterial lysates were cleared by high-speed centrifugation.

To purify the His-tagged proteins, the cleared bacterial lysates were incubated with nickel beads (Qiagen, Valencia, CA), prewashed, and equilibrated in PBS, with rotation for 2 h at 4°C. The resulting slurry of beads and lysates was centrifuged at 500 × *g* for 2 min at 4°C. The beads were washed four times with cold PBS, with 5-min rocking for every wash. The beads were further washed twice with PBS containing 20 mM imidazole and twice with PBS containing 50 mM imidazole. Slk19-His, Slk19-HA-His, or Slk19-Myc-His was then eluted at 4°C from the beads in PBS containing 100 mM Imidazole. The eluted proteins were then dialyzed in PBS at 4°C for 2 h. The purified proteins were stored at –80°C until used in the binding/dimerization assay. Samples of cleared bacterial lysates and purified proteins were analyzed on an SDS–PAGE gel and visualized with Coomassie blue staining. In addition, the expression of the HA and Myc tags was confirmed by Western blot analysis of the purified proteins with anti-HA and anti-Myc antibodies.

Slk19 binding/dimerization assays

For the binding assays, purified Slk19-HA-His was mixed with purified Slk19-Myc-His or Slk19-His (negative control) and incubated for 2 h at 4°C. The mixtures were then diluted with PBS up to 1 ml and incubated with anti-Myc antibody (Santa Cruz Biotechnology, Santa Cruz, CA) overnight at 4°C. Protein A/G beads were then added for 1 h. The protein-bead complexes were then pelleted by centrifugation at (1000 × g for 2 min at 4°C), washed four times with cold PBS, and boiled in 2× SDS–PAGE loading buffer before loading on the gel and subsequent Western blotting, as indicated in Figure 6B. This experiment was alternatively performed by incubating purified Slk19-Myc-His with purified Slk19-HA-His or Slk19-His (negative control), followed by immunoprecipitation with anti-HA antibody (Sigma-Aldrich).

ACKNOWLEDGMENTS

We thank Angelika Amon, Jeff Bachant, Frank Uhlmann, and Paul Megee for yeast strains and plasmids. We thank Xianying Tang, who constructed some of the yeast strains. We are grateful to Ruth Dider, who helped with live-cell imaging and superresolution microscopy. We also thank the members of the yeast community at Florida State University for reagents and suggestions. This work was supported by Research Scholar Grant RSG-08-104-010CCG from the American

Cancer Society, Grant R15GM097326-01 from the National Institutes of Health/National Institute of General Medical Sciences, and research grants from the College of Medicine at Florida State University to Y.W.

REFERENCES

Anderson M, Haase J, Yeh E, Bloom K (2009). Function and assembly of DNA looping, clustering, and microtubule attachment complexes within a eukaryotic kinetochore. Mol Biol Cell 20, 4131–4139.

Cohen-Fix O, Peters JM, Kirschner MW, Koshland D (1996). Anaphase initiation in *Saccharomyces cerevisiae* is controlled by the APC-dependent degradation of the anaphase inhibitor Pds1p. Genes Dev 10, 3081–3093.

Collins SR *et al*. (2007). Functional dissection of protein complexes involved in yeast chromosome biology using a genetic interaction map. Nature 446, 806–810.

De Wulf P, McAinsh AD, Sorger PK (2003). Hierarchical assembly of the budding yeast kinetochore from multiple subcomplexes. Genes Dev 17, 2902–2921.

Duan Z, Andronescu M, Schutz K, McIlwain S, Kim YJ, Lee C, Shendure J, Fields S, Blau CA, Noble WS (2009). A three-dimensional model of the yeast genome. Nature 465, 363–367.

Funabiki H, Hagan I, Uzawa S, Yanagida M (1993). Cell cycle-dependent specific positioning and clustering of centromeres and telomeres in fission yeast. J Cell Biol 121, 961–976.

Gardner MK *et al*. (2008). The microtubule-based motor Kar3 and plus end-binding protein Bim1 provide structural support for the anaphase spindle. J Cell Biol 180, 91–100.

Gillett ES, Espelin CW, Sorger PK (2004). Spindle checkpoint proteins and chromosome-microtubule attachment in budding yeast. J Cell Biol 164, 535–546.

Goh PY, Kilmartin JV (1993). NDC10: a gene involved in chromosome segregation in *Saccharomyces cerevisiae*. J Cell Biol 121, 503–512.

Goshima G, Yanagida M (2000). Establishing biorientation occurs with precocious separation of the sister kinetochores, but not the arms, in the early spindle of budding yeast. Cell 100, 619–633.

Havens KA, Gardner MK, Kamieniecki RJ, Dresser ME, Dawson DS (2010). Slk19p of *Saccharomyces cerevisiae* regulates anaphase spindle dynamics through two independent mechanisms. Genetics 186, 1247–1260.

He X, Asthana S, Sorger PK (2000). Transient sister chromatid separation and elastic deformation of chromosomes during mitosis in budding yeast. Cell 101, 763–775.

Holt SV, Vergnolle MA, Hussein D, Wozniak MJ, Allan VJ, Taylor SS (2005). Silencing Cenp-F weakens centromeric cohesion, prevents chromosome alignment and activates the spindle checkpoint. J Cell Sci 118, 4889–4900.

Indjeian VB, Murray AW (2007). Budding yeast mitotic chromosomes have an intrinsic bias to biorient on the spindle. Curr Biol 17, 1837–1846.

Indjeian VB, Stern BM, Murray AW (2005). The centromeric protein Sgo1 is required to sense lack of tension on mitotic chromosomes. Science 307, 130–133.

Janke C, Ortiz J, Lechner J, Shevchenko A, Magiera MM, Schramm C, Schiebel E (2001). The budding yeast proteins Spc24p and Spc25p interact with Ndc80p and Nuf2p at the kinetochore and are important for kinetochore clustering and checkpoint control. EMBO J 20, 777–791.

Jin F, Liu H, Li P, Yu HG, Wang Y (2012). Loss of function of the cik1/kar3 motor complex results in chromosomes with syntelic attachment that are sensed by the tension checkpoint. PLoS Genet 8, e1002492.

Jin F, Liu H, Liang F, Rizkallah R, Hurt MM, Wang Y (2008). Temporal control of the dephosphorylation of Cdk substrates by mitotic exit pathways in budding yeast. Proc Natl Acad Sci USA 105, 16177–16182.

Jin QW, Fuchs J, Loidl J (2000). Centromere clustering is a major determinant of yeast interphase nuclear organization. J Cell Sci 113, 1903–1912.

Khmelinskii A, Lawrence C, Roostalu J, Schiebel E (2007). Cdc14-regulated midzone assembly controls anaphase B. J Cell Biol 177, 981–993.

Kitamura E, Tanaka K, Kitamura Y, Tanaka TU (2007). Kinetochore microtubule interaction during S phase in *Saccharomyces cerevisiae*. Genes Dev 21, 3319–3330.

Kitamura E, Tanaka K, Komoto S, Kitamura Y, Antony C, Tanaka TU (2010). Kinetochores generate microtubules with distal plus ends: their roles and limited lifetime in mitosis. Dev Cell 18, 248–259.

Liang F, Wang Y (2007). DNA damage checkpoints inhibit mitotic exit by two different mechanisms. Mol Cell Biol 27, 5067–5078.

Liao H, Winkfein RJ, Mack G, Rattner JB, Yen TJ (1995). CENP-F is a protein of the nuclear matrix that assembles onto kinetochores at late G2 and is rapidly degraded after mitosis. J Cell Biol 130, 507–518.

Lin JJ, Zakian VA (1996). The *Saccharomyces* CDC13 protein is a single-strand TG1–3 telomeric DNA-binding protein in vitro that affects telomere behavior in vivo. Proc Natl Acad Sci USA 93, 13760–13765.

Liu H, Jin F, Liang F, Tian X, Wang Y (2011). The Cik1/Kar3 motor complex is required for the proper kinetochore-microtubule interaction after stressful DNA replication. Genetics 187, 397–407.

Liu H, Liang F, Jin F, Wang Y (2008). The coordination of centromere replication, spindle formation, and kinetochore-microtubule interaction in budding yeast. PLoS Genet 4, e1000262.

Lupas AN, Gruber M (2005). The structure of alpha-helical coiled coils. Adv Protein Chem 70, 37–78.

Mayer ML, Gygi SP, Aebersold R, Hieter P (2001). Identification of RFC(Ctf18p, Ctf8p, Dcc1p): an alternative RFC complex required for sister chromatid cohesion in *S. cerevisiae*. Mol Cell 7, 959–970.

Michaelis C, Ciosk R, Nasmyth K (1997). Cohesins: chromosomal proteins that prevent premature separation of sister chromatids. Cell 91, 35–45.

Newman JR, Wolf E, Kim PS (2000). A computationally directed screen identifying interacting coiled coils from *Saccharomyces cerevisiae*. Proc Natl Acad Sci USA 97, 13203–13208.

Ohkuni K, Abdulle R, Tong AH, Boone C, Kitagawa K (2008). Ybp2 associates with the central kinetochore of *Saccharomyces cerevisiae* and mediates proper mitotic progression. PLoS One 3, e1617.

Ortiz J, Funk C, Schafer A, Lechner J (2009). Stu1 inversely regulates kinetochore capture and spindle stability. Genes Dev 23, 2778–2791.

Pagliuca C, Draviam VM, Marco E, Sorger PK, De Wulf P (2009). Roles for the conserved spc105p/kre28p complex in kinetochore-microtubule binding and the spindle assembly checkpoint. PLoS One 4, e7640.

Pereira G, Schiebel E (2003). Separase regulates INCENP-Aurora B anaphase spindle function through Cdc14. Science 302, 2120–2124.

Pfiz S, Zimmermann J, Hilt W (2002). The yeast kinetochore protein Slk19 is required to prevent aberrant chromosome segregation in meiosis and mitosis. Genes Cells 7, 1033–1042.

Queralt E, Lehane C, Novak B, Uhlmann F (2006). Downregulation of PP2A(Cdc55) phosphatase by separase initiates mitotic exit in budding yeast. Cell 125, 719–732.

Rattner JB, Rao A, Fritzler MJ, Valencia DW, Yen TJ (1993). CENP-F is a .ca 400 kDa kinetochore protein that exhibits a cell-cycle dependent localization. Cell Motil Cytoskeleton 26, 214–226.

Sato M, Koonrugsa N, Toda T, Vardy L, Tournier S, Millar JB (2003). Deletion of Mia1/Alp7 activates Mad2-dependent spindle assembly checkpoint in fission yeast. Nat Cell Biol 5, 764–766.

Solovei I, Schermelleh L, During K, Engelhardt A, Stein S, Cremer C, Cremer T (2004). Differences in centromere positioning of cycling and postmitotic human cell types. Chromosoma 112, 410–423.

Stegmeier F, Visintin R, Amon A (2002). Separase, polo kinase, the kinetochore protein Slk19, and Spo12 function in a network that controls Cdc14 localization during early anaphase. Cell 108, 207–220.

Sullivan M, Lehane C, Uhlmann F (2001). Orchestrating anaphase and mitotic exit: separase cleavage and localization of Slk19. Nat Cell Biol 3, 771–777.

Sullivan M, Uhlmann F (2003). A non-proteolytic function of separase links the onset of anaphase to mitotic exit. Nat Cell Biol 5, 249–254.

Tanaka K, Kitamura E, Kitamura Y, Tanaka TU (2007). Molecular mechanisms of microtubule-dependent kinetochore transport toward spindle poles. J Cell Biol 178, 269–281.

Tanaka K, Mukae N, Dewar H, van Breugel M, James EK, Prescott AR, Antony C, Tanaka TU (2005). Molecular mechanisms of kinetochore capture by spindle microtubules. Nature 434, 987–994.

Tarassov K *et al*. (2008). An in vivo map of the yeast protein interactome. Science 320, 1465–1470.

Tong AH *et al*. (2004). Global mapping of the yeast genetic interaction network. Science 303, 808–813.

Vos LJ, Famulski JK, Chan GK (2006). How to build a centromere: from centromeric and pericentromeric chromatin to kinetochore assembly. Biochem Cell Biol 84, 619–639.

Wang Y, Ng TY (2006). Phosphatase 2A negatively regulates mitotic exit in *Saccharomyces cerevisiae*. Mol Biol Cell 17, 80–89.

Wargacki MM, Tay JC, Muller EG, Asbury CL, Davis TN (2010). Kip3, the yeast kinesin-8, is required for clustering of kinetochores at metaphase. Cell Cycle 9, 2581–2588.

Wong J *et al*. (2007). A protein interaction map of the mitotic spindle. Mol Biol Cell 18, 3800–3809.

Yang ZY, Guo J, Li N, Qian M, Wang SN, Zhu XL (2003). Mitosin/CENP-F is a conserved kinetochore protein subjected to cytoplasmic dynein-mediated poleward transport. Cell Res 13, 275–283.

Ye P, Peyser BD, Pan X, Boeke JD, Spencer FA, Bader JS (2005). Gene function prediction from congruent synthetic lethal interactions in yeast. Mol Syst Biol 1, 2005.0026.

Yeh E, Haase J, Paliulis LV, Joglekar A, Bond L, Bouck D, Salmon ED, Bloom KS (2008). Pericentric chromatin is organized into an intramolecular loop in mitosis. Curr Biol 18, 81–90.

Yellman CM, Burke DJ (2006). The role of Cdc55 in the spindle checkpoint is through regulation of mitotic exit in *Saccharomyces cerevisiae*. Mol Biol Cell 17, 658–666.

Zeng X, Kahana JA, Silver PA, Morphew MK, McIntosh JR, Fitch IT, Carbon J, Saunders WS (1999). Slk19p is a centromere protein that functions to stabilize mitotic spindles. J Cell Biol 146, 415–425.

Zhang T, Lim HH, Cheng CS, Surana U (2006). Deficiency of centromere-associated protein Slk19 causes premature nuclear migration and loss of centromeric elasticity. J Cell Sci 119, 519–531.

Zhu X, Chang KH, He D, Mancini MA, Brinkley WR, Lee WH (1995). The C terminus of mitosin is essential for its nuclear localization, centromere/kinetochore targeting, and dimerization. J Biol Chem 270, 19545–19550.